$PMo_{11}V$@N-CNT electrochemical properties and its application as electrochemical sensor for determination of acetaminophen

Diana M. Fernandes[1] · **Marta Nunes**[1] · **Belén Bachiller-Baeza**[2] · **Inmaculada Rodríguez-Ramos**[2] · **Antonio Guerrero-Ruiz**[3] · **Cristina Delerue-Matos**[4] · **Cristina Freire**[1]

Abstract A polyoxometalate-nanocarbon composite, $PMo_{11}V$@N-CNT, was prepared by a simple procedure which consisted of the immobilization of phosphovanadomolybdate ($PMo_{11}V$) onto N-doped carbon nanotubes (N-CNT). The FTIR and XPS characterizations confirmed its successful synthesis. The cyclic voltammograms of glassy carbon electrode (GCE) modified with $PMo_{11}V$ and $PMo_{11}V$@N-CNT showed four Mo-centred redox processes ($Mo^{VI/V}$) and a vanadium redox process ($V^{V/IV}$). All were surface-confined redox processes. Additionally, $PMo_{11}V$@N-CNT/GCE showed good stability and well-resolved redox peaks with high current intensities. The electrocatalytic sensing properties of $PMo_{11}V$@N-CNT/GCE towards acetaminophen (AC) in the presence of tryptophan (TRP) were evaluated by square wave voltammetry. Under the conditions used, the peak current increased linearly with AC concentration in the presence of TRP, with a linear range from 1.5×10^{-6} to 3.9×10^{-4} mol dm^{-3} and a detection limit of 1.0×10^{-6} mol dm^{-3}.

Keywords Phosphovanadomolybdates · N-doped carbon nanotubes · Electrocatalysis · Acetaminophen

Research highlights
- N-doped carbon nanotubes (N-CNT) functionalized with $PMo_{11}V$ were successfully prepared.
- The nanocomposite was successfully immobilized into GCE electrode.
- Modified electrode showed electrocatalytic activity for acetaminophen oxidation.

Electronic supplementary material The online version of this article (doi:10.1007/s10008-016-3463-5) contains supplementary material, which is available to authorized users.

✉ Diana M. Fernandes
diana.fernandes@fc.up.pt

✉ Cristina Freire
acfreire@fc.up.pt

[1] REQUIMTE/LAQV, Departamento de Química e Bioquímica, Faculdade de Ciências, Universidade do Porto, 4169-007 Porto, Portugal

[2] Instituto de Catálisis y Petroleoquímica, CSIC, C/ Marie Curie 2, Cantoblanco, 28049 Madrid, Spain

[3] Departamento de Química Inorgánica y Química Técnica, Facultad de Ciencias, UNED, Senda del Rey 9, 28040 Madrid, Spain

[4] REQUIMTE/LAQV, Instituto Superior de Engenharia do Porto, Instituto Politécnico do Porto, 4200-072 Porto, Portugal

Introduction

In order to develop electrochemical sensors with higher performances, the modification of numerous electrode surfaces has been a major focus of research. Different modified electrodes have been prepared using several types of routes. This can be achieved through film growing at the electrode surface by layer-by-layer technique or by electrodeposition using highly redox-active molecular compounds and polyelectrolytes and/or polymers. Another highly popular method is the deposition on the electrode surface of hybrid composite (nano)materials that result from the integration of redox-active species into sophisticated conductive materials, giving rise to compounds with extraordinary versatility and enhanced performances [1, 2]. An excellent example of conductive nanostructured phases are the carbon-based materials, such as graphene and carbon nanotubes (CNTs).

CNTs were discovered in 1991 by Iijima [3] and are one-dimensional materials, consisting of cylinder(s) of graphite layer(s), that may exist as single-walled (SWCNT) or multi-walled (MWCNT) carbon nanotubes [4]. These materials are highly used in the modification of electrodes especially due to their availability, cost-effectiveness and excellent

physicochemical and electrochemical properties. Their large surface area, high electrical conductivity and mechanical strength, chemical stability and wide potential window can be highlighted [5]. As a result, CNTs have found several potential applications, namely in energy-related systems [6, 7] and in electrochemical sensing [8–13]. It is worth mentioning that, in all cases, the CNTs can act either as the electrocatalyst support or as the electrocatalyst itself. Generally, the CNT-based sensors have the advantage of showing higher selectivity and sensitivity, lower detection limits and resistance to surface fouling and to passivation [10].

More recently, it has been reported that the chemical doping of CNTs with heteroatoms (e.g. nitrogen and/or boron) can dramatically change their chemical and electrical properties. Nitrogen is considered to be one of the best dopants because its atomic radius is close to that of carbon. Furthermore, N-doping creates an electron donor in the conduction band (n-type dopant), which leads to noteworthy modifications in electrical conductivity and chemical reactivity [14]. The CNT doping with nitrogen (CNT-N) can contribute to improve their intrinsic electrocatalytic activity, and when used as support, this type of doping can enhance the interaction between the CNT support and the catalyst, creating a new catalytic system with better performance [15, 16] .

Polyoxometalates (POMs) are an important class of metal oxygen clusters of early transition elements, with several important properties such as high chemical and structural versatility, robustness to oxidative degradation, high thermal stability and their solubility depends essentially on the countercation used, which make them promising building blocks for nanocomposites [1]. Simultaneously, the POM framework can undergo reversible and stepwise multi-electron transfer reactions without decomposition, mainly due to the fact that their essential constituents (Mo and W) are in their higher oxidation state, making them attractive candidates to electrocatalysis [17]. Taking into account all these characteristics, the incorporation of POMs into CNTs can be very appealing. In fact, several POM@CNT nanocomposite-modified electrodes have been reported [18], with application mainly in charge-discharge phenomena [19], energy storage [20], molecular cluster batteries [21], lithium-ion batteries [22, 23], capacitors [24, 25] and electrocatalysis [18, 26, 27]. Several POMs have also been immobilized on metal-organic frameworks [28, 29], nitrogen-doped graphene [30] and, inclusively, on single-walled carbon nanotubes [26] to nitrite and iodate reduction, ascorbic acid oxidation and dopamine, acetaminophen and theophylline sensing, which shows the wide range of POM electrocatalytic action.

Acetaminophen (paracetamol, AC) is the most widely used analgesic and antipyretic drug in the world, usually used for pain relief and fever [31, 32]. When used appropriately, the side effects are rare but overdoses of AC can cause liver and kidney damage and possibly mortality [33]. Consequently, the determination of AC alone and/or in mixtures is important to control not only the quality of pharmaceutical formulations but also their amount in biological fluids (blood and urine) [34–36]. Tryptophan (TRP) is one of the 20 essential amino acids for the human body and an important constituent of protein biosynthesis of living organisms [31, 37]. As the human body cannot produce TRP, it is sometimes added to dietary and feed products as a food fortifier and to pharmaceutical formulations in order to correct possible dietary deficiencies [33]. The major problem with TRP is due to the occurrence of its improper metalobization which results in the formation of toxic by-products in the brain, causing hallucination and delusions [37]. The metabolism of TRP is affected by the presence of AC, and so, the development of modified electrodes for the electrochemical detection of these compounds is a very useful tool [32, 38, 39].

This work reports the preparation of a new nanocomposite, designated $PMo_{11}V$@CNT-N, by the immobilization of the tetrabutylammonium salt of phosphovanadomolybdate $[PMo_{11}VO_{40}]^{5-}$ ($PMo_{11}V$) into nitrogen-doped carbon nanotubes (CNT-N). The nanocomposite was evaluated with success, as an electrochemical sensor, in the detection of acetaminophen in the presence of tryptophan.

Experimental section

Materials and instrumentation

The N-CNT nanomaterial was prepared by catalytic chemical vapour decomposition according to the procedure reported in reference [40]. The N content of the N-CNT sample was 4.1% and was determined by elemental analysis with a LECO CHNS-932 system. The POM was prepared using a procedure described in the literature [41] and characterized by numerous techniques, and the $PMo_{11}V$@N-CNT was prepared using an adapted procedure [26].

Tryptophan (Fluka), acetaminophen (Sigma-Aldrich, >99) and acetonitrile (Romil) were used as received. The spectrophotometer used to acquire the FTIR spectra was a Jasco FT/IR-460 Plus, and the spectra were obtained in KBr pellets (249.5 mg) containing 0.5 mg of $PMo_{11}V$@N-CNT.

A VG Scientific ESCALAB 200A spectrometer using non-monochromatized Al Kα radiation (1486.6 eV) was used for X-ray photoelectron spectroscopy (XPS) measurements at CEMUP (Porto, Portugal). The correction of eventual deviations was performed using the C 1 s band at 285.0 eV as the internal standard. The software used to deconvolute the XPS spectra was the XPSPEAK 4.1. Scanning electron microscopy (SEM) was carried out using a high-resolution (Schottky) environmental SEM with X-ray microanalysis and backscattered electron

diffraction pattern analysis (FEI Quanta 400FEG/EDAX Genesis X4M), in high-vacuum conditions, at the Centro de Materiais da Universidade do Porto (CEMUP).

Electrochemical measurements

For the electrochemical studies either by cyclic voltammetry (CV) or square-wave voltammetry (SWV), an Autolab PGSTAT 30 potentiostat/galvanostat (EcoChimie B.V.) controlled by a GPES software was used. The system used was a three-electrode cell: working—glassy carbon electrode, GCE, (d = 3 mm diameter); auxiliary—platinum wire (7.5 cm); reference—Ag/AgCl (sat. KCl). All studies were carried out at room temperature, and before every experiment, the solutions were purged with nitrogen.

For the electrochemical studies, a H_2SO_4/Na_2SO_4 buffer solution (pH 2.5) was used. All the electrolyte solutions were prepared using ultra-pure water (resistivity 18.2 MΩ cm at 25 °C, Millipore).

The dispersion used to modify the electrodes consisted in 1 mg of N-CNT or $PMo_{11}V$@N-CNT in 3 mL of *N*,*N*-dimethylformamide (DMF) which was sonicated for 10 min. For the $PMo_{11}V$ solution, 1 mg of compound was dissolved in 1 mL of DMF.

Before any experiment or modification, the electrode was carefully cleaned: polished using diamond pastes of 6, 3 and 1 μm followed by aluminium oxide (0.3 μm) on a polishing pad. Then the GCE was washed with ultra-pure water and finally sonicated for 5 min in ultra-pure water. The GCE modification was achieved through drop casting using a 3-μL drop of the appropriate dispersion/solution. The solvent was evaporated under an air flow.

Results and discussion

Nanocomposite preparation and characterization

The TBA-$PMo_{11}V$ was prepared according to our previously work and characterized by NMR spectroscopy (^{31}P and ^{51}V) and FTIR. The NMR spectra (data not shown) presented one peak at −4.6 eV for ^{31}P and one at −525.4 eV for ^{51} V, confirming successful POM synthesis [26]. The FTIR spectra of TBA-$PMo_{11}V$ as well as those of N-CNT and $PMo_{11}V$@N-CNT are shown in Fig. 1. As can be observed, in the TBA-$PMo_{11}V$ spectrum, the typical POM bands at 2871 and 2960 cm^{-1} (C–H stretching vibration), 1479 and 1374 cm^{-1} (C–H bending vibration), two bands in the interval 1080–1040 cm^{-1} (splitting of the P–O stretching vibration), 945 cm^{-1} (Mo–O_d vibration), 872 cm^{-1} (Mo–O_b–Mo) and 799 cm^{-1} (Mo–O_c–Mo) are present [26, 41]. In Fig. 1a, the spectrum of N-CNT where weak and poorly resolved vibrational bands are observed is shown: 3420, 1560, 1385 and 1160 cm^{-1}. The first is assigned to the stretching vibrations of the OH groups, the second to C=N stretching vibrations or C=C stretching vibrations of the aromatic carbon [42] and the latter two are attributed to C–N and C–O stretching vibration, respectively [26, 43].

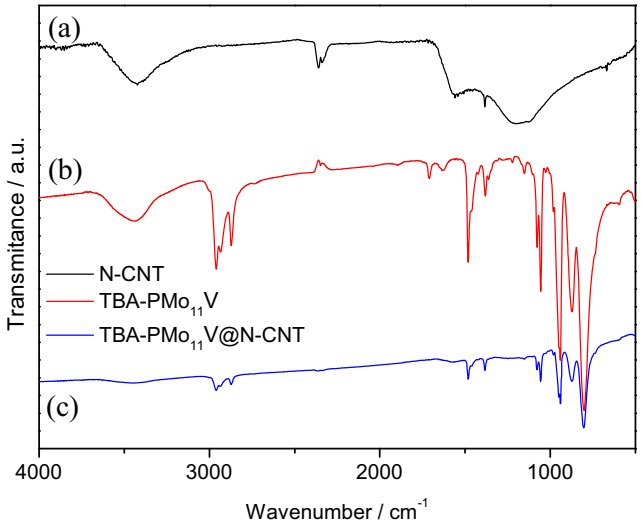

Fig. 1 FTIR spectra in the range 4000–500 cm^{-1} for N-CNT (**a**), $PMo_{11}V$ (**b**) and $PMo_{11}V$@N-CNT (**c**)

The final nanocomposite $PMo_{11}V$@N-CNT was also characterized by FTIR, which confirmed the successful immobilization of TBA-$PMo_{11}V$ onto N-CNT through the existence of the bands due to N-CNT in the range of 1120–1580 cm^{-1} and the vibrational bands assigned to POM in the range of 798–1081 cm^{-1} and TBA at 2956, 2868, 1478 and 1380 cm^{-1}.

All materials were also characterized by XPS, and the spectrum of $PMo_{11}V$@N-CNT can be observed in Fig. 2 and of N-CNT in Figure S1 (see Supporting Information, SI). In Table 1, the surface atomic percentages of each component in both materials are presented and the obtained binding energies are in Table S1 (see SI). The final nanomaterial presents all elements of each component: C, O, N from N-CNT and P, Mo, O, N, V from the POM, which confirms the successful fabrication of the nanocomposite. The atomic ratios of ≈1:11 and 1:1 for V/Mo and P/V, respectively, suggest that the integrity of the POM arrangement is maintained after its immobilization.

The C 1 s spectrum of pristine N-CNT (Figure S1(a), SI) was fitted with six peaks at: 285.0 eV—graphitic structure (sp^2) (major peak), 286.2 eV—C–C and C–N, 286.9 eV—C–O, 287.8 eV—C=O, 288.9 eV—−COO and the peak at 291.0—shake-up satellite for the π–π^* transition [44, 45]. For $PMo_{11}V$@N-CNT, the C 1 s spectrum (Fig. 2a) was also fitted with six peaks: 285.0, 286.2, 287.1, 287.9, 288.6 and 290.3 eV with the same assignment as for N-CNT. The peak at 286.2 eV presented an increase, which is due to the tetrabutyl groups from the salt.

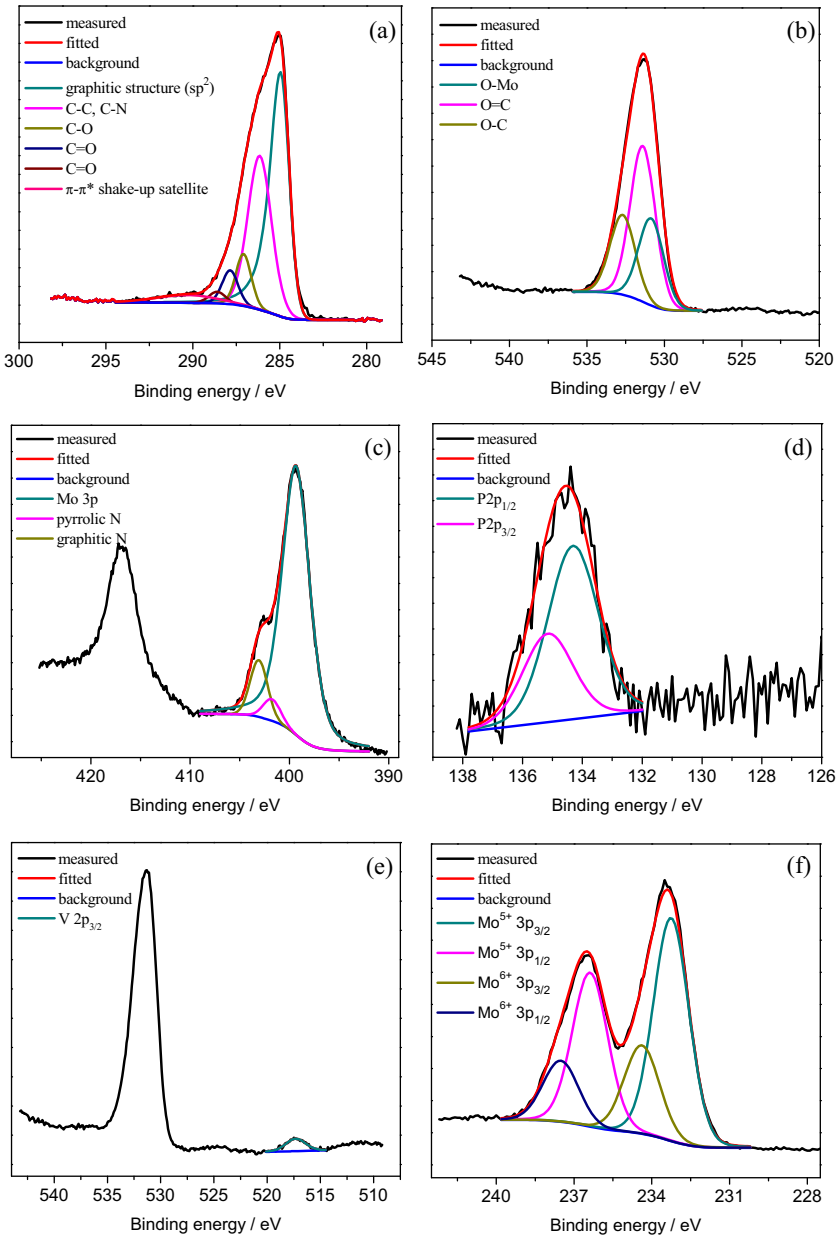

Fig. 2 Deconvoluted C 1 s (**a**), O 1 s (**b**), N 1 s (**c**), P 2p (**d**), Mo 3d (**e**) and V 2p (**f**) XPS spectra of $PMo_{11}V$@N-CNT

Also for the N-CNT, the O 1 s high-resolution spectrum was fitted with two peaks at 531.1 and 533.3 eV attributed to O═C (ketone, quinone moieties) and to O–C from ether and phenol groups, respectively. The $PMo_{11}V$@N-CNT O 1 s spectrum was deconvoluted into three peaks with binding energies at 530.8, 531.4 and 532.7 eV. The first peak is ascribed to O-Mo [26], and the last two are assigned as described for N-CNT.

Table 1 XPS surface atomic percentages for N-CNT and $PMo_{11}V$@N-CNT

Sample	Atomic %[a]					
	C 1 s	O 1 s	N 1 s	P 2p	V 2p	Mo 3d
N-CNT	80.1	9.8	10.1			
PMo_1V@N-CNT	70.5	19.8	3.3	0.5	0.5	5.4

[a] Determined by the areas of the respective bands in the high-resolution XPS spectra

The N 1 s XPS spectrum of N-CNT was deconvoluted into five peaks: 399.1, 401.5, 404.1, 406.5 and 409.6 eV attributed to pyridinic-N, pyrrolic-N, graphitic N, pyridinic N^+–O^- and some oxidized N, respectively [46, 47]. For the final composite ($PMo_{11}V$@N-CNT), the presence of N could be evaluated, but for the atomic percentage determination, we had to take into account the overlapping of the Mo 3p and N 1 s peaks, so the spectrum was fitted considering the existence of the Mo 3p and N

Table 2 Core-level binding energies of each component for N-CNT and $PMo_{11}V$@N-CNT obtained by curve fitting of XPS spectra

Sample	Binding energy (BE)[a]					
	C 1 s	O 1 s	N 1 s	P $2p_{3/2} + 3p_{1/2}$	V $2p^{3/2}$	Mo $3d_{3/2} + 3d_{5/2}$ (Mo^{6+}/Mo^{5+})
N-CNT	285.0 (0.99), 286.2 (1.08), 286.9 (1.13), 287.8 (1.38), 288.9 (1.38), 291.0 (3.8)	531.1 (2.37), 533.3 (2.37)	399.1 (2.40), 401.5 (2.40), 404.1 (2.40), 406.5 (2.40), 409.6 (2.40)			
$PMo_{11}V$@N-CNT	285.0 (1.17), 286.2 (1.60), 287.1 (1.03), 287.9 (1.07), 288.6 (1.13), 290.3 (4.00)	530.8 (1.91) 531.4 (1.91), 532.7 (1.91)	401.8 (2.10), 403.1 (2.10)	134.3 (1.99), 135.2 (1.99)	517.3 (2.19)	234.4 (1.61), 237.5 (1.61), 233.2 (1.61), 236.4 (1.61)

[a] The values between brackets refer to the FWHM of the bands

1 s peaks. The area obtained through modulation of Mo 3p was compared with the one obtained for Mo 3d, and it was practically the same, suggesting that the fitting of peaks considering the N 1 s peaks was right. The two peaks in the N 1 s spectrum at 401.8 and 403.1 eV were attributed to pyridinic and pyrrolic-N, respectively.

The Mo 3d XPS spectrum of $PMo_{11}V$@N-CNT was fitted with two couples of peaks: 233.2 and 236.4 eV assigned to Mo^{5+} and 234.4 and 237.5 eV allocated to Mo^{6+}. The higher quantity of Mo^{5+} species (atomic % of 3.8) in comparison with that for Mo^{6+} (atomic % of 1.6) suggests that a significant photoreduction of POM occurred. This could have happened during the nanocomposite preparation or when it was exposed to the X-ray source as Mo-polyoxometalates are easily reduced by external factors such as radiation, high pressures and heat. Nevertheless, as their redox processes are reversible, if these factors are stopped, they return to the original state (Table 2).

The image obtained by SEM of the $PMo_{11}V$@N-CNT (Fig. 3) revealed that the N-doped carbon nanotubes are decorated with light micro-sized spots that correspond to polyoxometalate aggregates. The EDX spectrum of composite material confirms the existence of Mo, V and P from the polyoxomolybdate and N belonging to the N-CNT, as well as the elemental mapping analysis revealed homogeneous distribution of all these elements in the composite material confirming the uniform incorporation of the $PMo_{11}V$ into the N-CNT (Fig. 3).

Materials electrochemical characterization

Prior to the nanocomposite electrochemical behaviour studies, the electroactive surface area of bare GCE and modified electrodes (N-CNT/GCE and $PMo_{11}V$@N-CNT/GCE) were evaluated. These were determined from the CVs of 1×10^{-3} mol dm^{-3} $K_3[Fe(CN)_6]$ in 1 mol dm^{-3} KCl (Fig. S2, SI) using the Randles-Sevcik equation (Eq. 1) and assuming that electrode processes are controlled by diffusion:

$$i_{pa} = 2.69 \times 10^5 n^{3/2} A D_r^{1/2} R_\infty v^{1/2} \quad (1)$$

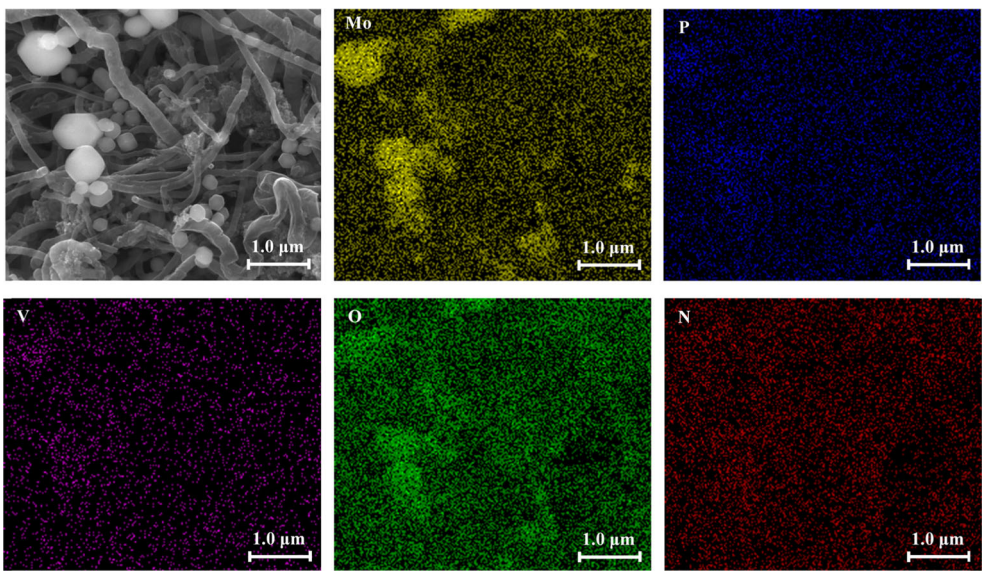

Fig. 3 SEM and EDX elemental mapping images for $PMo_{11}V$@N-CNT

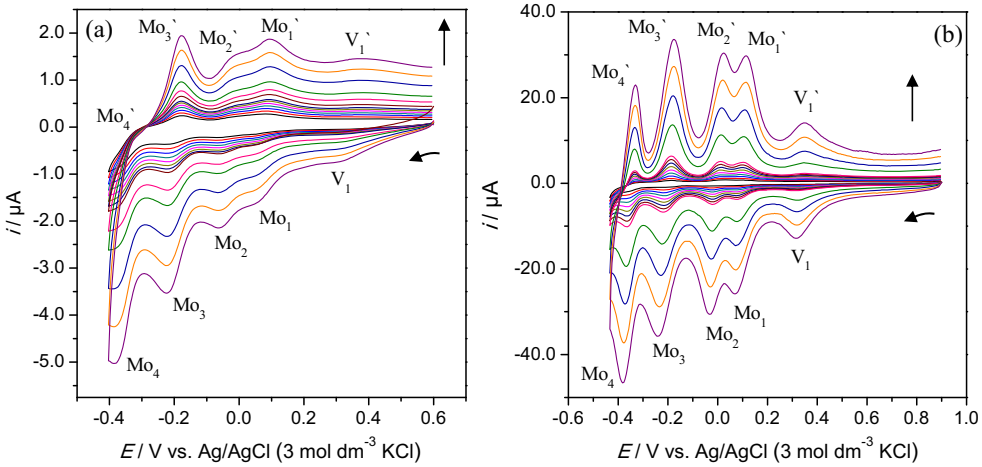

Fig. 4 Cyclic voltammograms in pH 2.5 H_2SO_4/Na_2SO_4 buffer solution at different scan rates from 0.02 to 0.5 V s^{-1} of $PMo_{11}V$ (**a**) and $PMo_{11}V$@N-CNT (**b**)

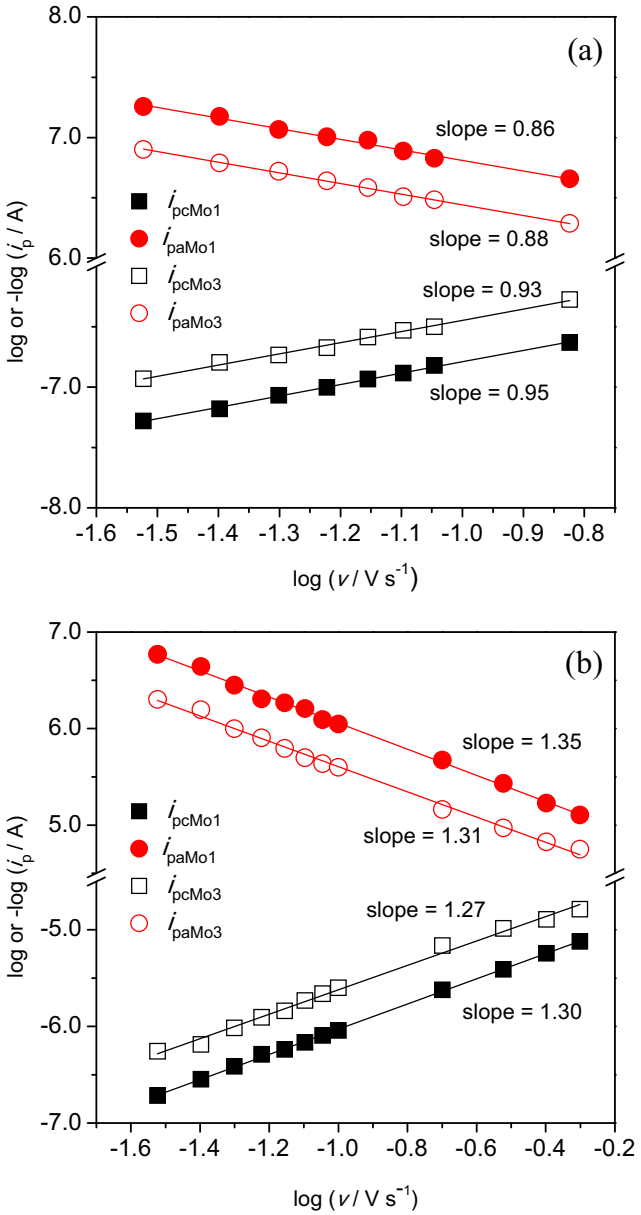

Fig. 5 Plots of log (i_{pc} / A) and i_{pa} vs. log (ν / Vs^{-1}) of $PMo_{11}V$ (**a**) and $PMo_{11}V$@N-CNT (**b**)

where i_{pa} is the intensity of the anodic peak current (A), ν is the scan rate (V s^{-1}), the electrons involved in this process, n, is one, A is the electrode surface area (cm^2), D_r is the diffusion coefficient (7.6×10^{-6} cm^2 s^{-1}) and R_∞ is the concentration of the species (mol cm^{-3}) [36]. The A values obtained were: 0.0443, 0.0484 and 0.0595 cm^2 for bare GCE, N-CNT/GCE and $PMo_{11}V$@N-CNT/GCE, respectively. This means that when the electrode is modified with N-CNT, the electroactive surface area increases ≈9 %, and if the modifier is $PMo_{11}V$@N-CNT, the increase is close to 34%. This suggests a better pathway for the electron-transfer of $[Fe(CN)_6]^{3-/4-}$ in the latter electrode. Also, the peak-to-peak separations (ΔE_p) vary between 0.072 and 0.094 V for GCE, 0.077 and 0.111 V for N-CNT/GCE and 0.090 and 0.184 V for $PMo_{11}V$@N-CNT/GCE for the lowest (0.020 V s^{-1}) and highest (0.50 V s^{-1}) scan rates used.

The electrochemical performance of $PMo_{11}V$/GCE and $PMo_{11}V$@N-CNT/GCE was studied in pH 2.5 H_2SO_4/Na_2SO_4 buffer solution (Fig. 4). The CVs obtained for $PMo_{11}V$/GCE show five redox processes, symbolized as V_1 and Mo_1 to Mo_4, Fig. 4a: E_{pcV1} = 0.311 V, E_{pcMo1} = 0.056 V, E_{pcMo2} = −0.058 V, E_{pcMo3} = −0.181 V and E_{pcMo4} = −0.376 V vs. Ag/AgCl. The peak at more positive potentials (V_1) is assigned to a one-electron vanadium redox process ($V^V \rightarrow V^{IV}$) while the peaks Mo_1 to Mo_4 are ascribed to four molybdenum redox processes (2 $Mo^{VI} \rightarrow 2$ Mo^V).

The CVs for $PMo_{11}V$@N-CNT/GCE (Fig. 4b) also shows five redox processes: E_{pcV1} = 0.318 V, E_{pcMo1} = 0.072 V, E_{pcMo2} = −0.018 V, E_{pcMo3} = −0.216 V and E_{pcMo4} = −0.364 V vs. Ag/AgCl. Nevertheless, compared with the POM/GCE, all the peaks are much better resolved and have higher current intensities (≈20 times higher). This suggests faster electron-transfer kinetics, which is related with the unique electronic property of the N-doped carbon nanotubes. The scan rate effect was also evaluated, and in the range 0.02 to 0.5 V s^{-1}, both cathodic (E_{pc}) and anodic (E_{pa}) peak potentials varied less than 0.011 V for $PMo_{11}V$ and 0.010 V

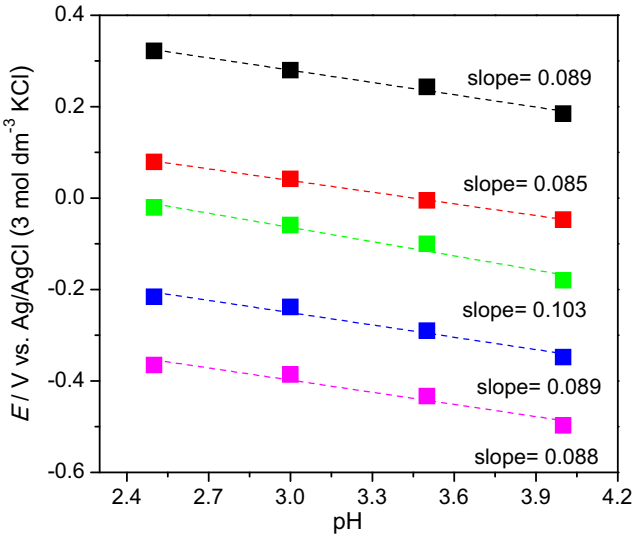

Fig. 6 Plots of E_p versus pH of $PMo_{11}V$@N-CNT/GCE, scan rate 0.050 V s^{-1}

for $PMo_{11}V$@N-CNT. The plots of log i_p versus log v for the Mo_1 and Mo_3 waves of $PMo_{11}V$/GCE and $PMo_{11}V$@N-CNT/GCE are shown, as example, in Fig. 5. Both i_{pc} and i_{pa} are directly proportional to the scan rate for all peaks, with $0.998 \geq r^2 \geq 0.991$ for $PMo_{11}V$ and $0.999 \geq r^2 \geq 0.993$ for $PMo_{11}V$@N-CNT, which indicate surface-confined processes [26]. The ΔE_p of all redox processes vary between 0.028 (0.02 V s^{-1}) and 0.057 V (0.5 V s^{-1}), and the ratios i_{pa}/i_{pc} are close to one (0.96 ± 0.05).

The equation $\Gamma = (4i_pRT)/(n^2F^2\nu A)$ was used to estimate the electrochemical surface coverages $PMo_{11}V$/GCE and $PMo_{11}V$@N-CNT/GCE, where i_p is the peak current (A), $n = 2$ (number of electrons transferred), ν is the scan rate (V s^{-1}), $A = 0.07065$ cm^2 (geometric area of GCE), R is the gas constant, $T = 298$ K and F is Faraday's constant. Peak currents of Mo_1 were plotted against ν, and the value of i_p/ν obtained was used to calculate the electrochemical surface coverage: 0.006 nmol cm^{-2} for $PMo_{11}V$ and 0.092 nmol cm^{-2} for $PMo_{11}V$@N-CNT. The modification with $PMo_{11}V$@N-CNT leads to an electrochemical surface coverage 15 times higher than that obtained for $PMo_{11}V$. This increase is a consequence of the high surface area of N-CNT which allowed the presence at the GCE surface of greater quantity of the electroactive $PMo_{11}V$.

The pH of the electrolyte solution effect was also evaluated. In Fig. 6, the plots of E_p vs. pH for $PMo_{11}V$@N-CNT/GCE are depicted. The results show that all the redox processes present a marked dependence of E_p and i_p with pH: the increase of pH, from 2.5 to 4.0, shifts the peak potentials to more negative values, while the peak currents gradually decrease. The reduction increases the negative charge density at the heteropolyanion and, thus, its basicity. As a consequence, the reduction is accompanied by protonation. The dependence of E_p vs. pH corresponds to straight lines that show slopes between 0.083 and 0.103 V/pH unit ($0.997 \geq r \geq 0.949$), which indicates that the redox processes require the involvement of protons. In the experimental conditions used and assuming a Nernstian behaviour, the V-based reduction corresponds to a one-electron/two proton process while the Mo-based reductions correspond to two-electron/three proton processes [26, 48].

Electrocatalytic sensing performance of nanocomposite modified electrodes

The electrochemical oxidation of acetaminophen (AC) and tryptophan (TRP) was first studied individually by SWV at the three different electrodes. Figure 7 shows the CVs of 5.0×10^{-4} mol dm^{-3} solutions of AC and TRP at a bare (i) and modified GCE (N-CNT (ii) and $PMo_{11}V$@N-CNT (iii)). At the bare GCE electrode, the oxidation peaks of AC and TRP are observed at ≈0.624 V and at ≈1.012 V vs. Ag/AgCl, respectively.

At an N-CNT-modified electrode, the oxidation peak of AC shifts to more positive potentials (0.675 V) and the peak current decreases approximately 20%. However, for the

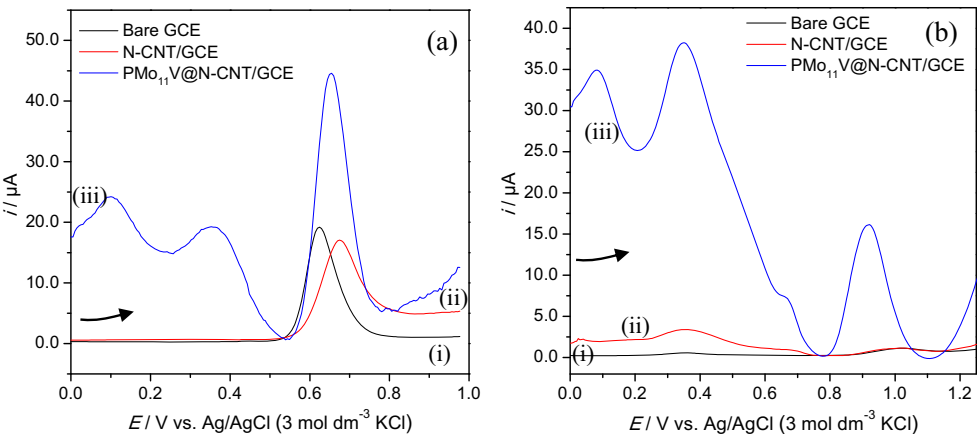

Fig. 7 Square wave voltammograms of 5.0×10^{-4} mol dm^{-3} AC (**a**) and TRP (**b**) at a bare GCE, N-CNT/GCE and $PMo_{11}V$@N-CNT/GCE in pH 2.5 H_2SO_4/Na_2SO_4 buffer solution, scan rate 0.050 V s^{-1}

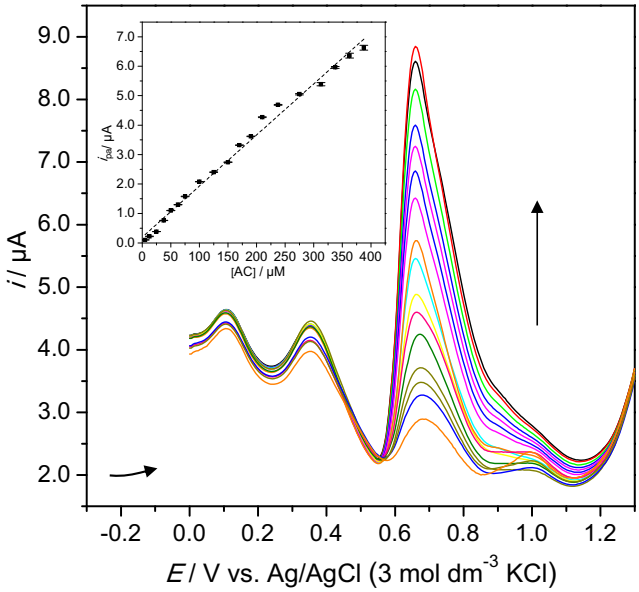

Fig. 8 Square-wave voltammetric response at a $PMo_{11}V$@N-CNT/GCE in pH 2.5 buffer solution containing 1.0×10^{-4} mol dm^{-3} TRP and different concentrations of AC from 1.5×10^{-6} to 3.9×10^{-4} mol dm^{-3}. *Inset*: plots of the anodic peak current as a function of the AC concentration

$PMo_{11}V$@N-CNT-modified electrode, the peak current increases ≈127% when compared with that obtained with a bare GCE, and the peak potential shifts only 0.031 V. These variations suggest that the $PMo_{11}V$@N-CNT composite material has a strong interaction with the AC species, leading to a better detection.

The TRP peak appears at almost the same potential when the N-CNT/GCE is used (change of 0.010 V) and the peak currents only increase ≈3%. More significant results were obtained for $PMo_{11}V$@N-FLG/GCE: E_{pa} cathodic shift of 0.091 V and i_p of 2586%, suggesting that this modified electrode is very sensitive to the presence of TRP.

Determination of AC in the presence of TRP at a $PMo_{11}V$@N-CNT/GCE

Figure 8 shows selected SWV obtained for the addition of increasing amounts of AC. The i_{pa} of AC increases linearly ($i = 0.017 \pm 0.001\ c_{AC} + 0.20$, $r^2 = 0.991$) with the increasing concentration of AC from 1.5×10^{-6} to 3.9×10^{-4} mol dm^{-3} in the presence of TRP (inset in Fig. 8), leading to a detection limit (DL) of 1.0×10^{-6} mol dm^{-3} (DL = 3σ/slope, with σ = standard deviation of the blank).

The use of this type of POM or POM-based nanocomposites for the determination of biomolecules is scarce, and most examples concern their application towards dopamine and ascorbic acid with good results compared to other more expensive solutions [26]. As far as we know, these have never been used for acetaminophen determination. Nevertheless, the obtained DL in this work is very close to that reported (0.83×10^{-6} mol dm^{-3}) for a similar study with a $MnFe_2O_4$@N-CNT [36] nanocomposite or with other carbon-based modified electrodes (Table 3) [32, 49, 50] and better than those obtained for poly(thionine) and poly(methylene green)/multi-walled carbon nanotube (MWCNT) modified electrodes [51, 52]. The only sensor with better results was the N-MWCNTs/AuNPs [53] with a DF = 0.35×10^{-6} mol dm^{-3}; however, this involved the use of gold nanoparticles which is less cost-effective and requires more complex sensor architecture.

Table 3 The detection limits and linear ranges of different modified electrodes for the determination of AC

Electrode materials	Detection limit ($\times 10^{-6}$ mol dm^{-3})[a]	Linear range ($\times 10^{-6}$ mol dm^{-3})	Reference
$PMo_{11}V$@N-CNT /GCE	1.0	1.5–390	This work
$MnFe_2O_4$@N-CNT/GCE	0.83	1–100	[36]
NiO–CuO/GR/GCE	1.23	4–400	[32]
C-Ni/GCE[b]	2.3	7.8 – 110	[49]
Lt/fMWCNT/GCE[c]	0.78	0.9–80	[50]
PTH/MWCNT/CFE[d]	6.0	25–250	[52]
MWCNT/PTH/CFE[d]	4.7	25–250	[52]
N-MWCNTs/AuNPs[e]	0.35	0.063 – 190	[53]
PMG/fMWCNT/GrCE[f]	4.3	25 – 200	[51]

[a] Detection limit(DL) = 3σ/slope, where σ is the standard deviation of the blank

[b] carbon-coated nickel magnetic nanoparticles

[c] luteolin functionalized multi-walled carbon nanotubes (MWCNT)

[d] MWCNT/poly(thionine) (PTH) nanostructures

[e] nitrogen-doped MWCNT modified with gold nanoparticles

[f] PMG poly(methylene green)

Finally, the stability of the $PMo_{11}V$@N-CNT/GCE was evaluated by measuring and comparing the i_{pa} of 0.5 mM AC in pH 2.5 H_2SO_4/Na_2SO_4 (pH 2.5) at the beginning and at the end of all set of experiments (data not shown). The E_p did not change, and the i_p only decreased by 2%, which confirms the electrochemical stability of the proposed modified electrode.

Conclusions

The phosphovanadomolybdate $PMo_{11}V$ was successfully immobilized on N-doped carbon nanotubes. XPS revealed that the POM structure was kept in the final nanocomposite. The preparation of modified electrodes with $PMo_{11}V$@N-CNT was easy, fast and reproducible and leads to stable electrodes. $PMo_{11}V$@N-CNT/GCE revealed five well-defined, surface-confined redox processes that were attributed to 4 Mo centres ($Mo^{VI} \rightarrow Mo^{V}$) and a V centre ($V^{V} \rightarrow V^{IV}$). The study of pH effect revealed that all electrochemical processes required the involvement of protons. The electrochemical surface coverage obtained for $PMo_{11}V$@N-CNT nanocomposite was 15 times higher compared to $PMo_{11}V$, which constitutes an outstanding advantage for electrocatalytic applications: $PMo_{11}V$@N-CNT showed good electrocatalytic sensing properties towards AC and TRP oxidations and allowed the detection of AC in the presence of an excess of TRP.

Acknowledgements The Fundação para a Ciência e a Tecnologia (FCT), FEDER under Programme PT2020 (Project UID/QUI/50006/2013) and Programme FCT–UT Austin, Emerging Technologies (Project UTAP-ICDT/CTM-NAN/0025/2014) is acknowledged for the financial funding. DF (SFRH/BPD/74877/2010) and MN (SFRH/BD/79171/2011) also thank FCT for their grants. Thanks are also due to COST Action CM-1203 PoCheMoN.

References

1. Genovese M, Lian K (2015) Polyoxometalate modified inorganic-organic nanocomposite materials for energy storage applications: a review. Curr Opin Solid State Mat Sci 19(2):126–137
2. Zen JM, Kumar AS, Tsai DM (2003) Recent updates of chemically modified electrodes in analytical chemistry. Electroanal 15(13): 1073–1087
3. Iijima S (1991) Helical microtubules of graphitic carbon. Nature 354:56–58
4. Trogadas P, Fuller TF, Strasser P (2014) Carbon as catalyst and support for electrochemical energy conversion. Carbon 75:5–42
5. Mao XW, Rutledge GC, Hatton TA (2014) Nanocarbon-based electrochemical systems for sensing, electrocatalysis, and energy storage. Nano Today 9(4):405–432
6. Zhou M, Wang HL, Guo SJ (2016) Towards high-efficiency nanoelectrocatalysts for oxygen reduction through engineering advanced carbon nanomaterials. Chem Soc Rev 45(5):1273–1307
7. Danilov MO, Kolbasov GY (2010) Electrochemical method for the preparation nanocomposites based on carbon nanotubes and chromium oxides for oxygen electrodes. J Solid State Electrochem 14(12):2169–2172
8. Gutierrez A, Gasnier A, Pedano ML, Gonzalez-Dominguez JM, Anson-Casaos A, Hernandez-Ferrer J, Galicia L, Rubianes MD, Martinez MT, Rivas GA (2015) Electrochemical sensor for the quantification of dopamine using glassy carbon electrodes modified with single-wall carbon nanotubes covalently functionalized with Polylysine. Electroanal 27(7):1565–1571
9. Merkoci A, Pumera M, Llopis X, Perez B, del Valle M, Alegret S (2005) New materials for electrochemical sensing VI: carbon nanotubes. Trac-Trends Anal Chem 24(9):826–838
10. Balasubramanian K, Burghard M (2006) Biosensors based on carbon nanotubes. Anal Bioanal Chem 385(3):452–468
11. Akhgar MR, Salari M, Zamani H (2011) Simultaneous determination of levodopa, NADH, and tryptophan using carbon paste electrode modified with carbon nanotubes and ferrocenedicarboxylic acid. J Solid State Electrochem 15(4):845–853
12. Kharian S, Teymoori N, Khalilzadeh MA (2012) Multi-wall carbon nanotubes and TiO2 as a sensor for electrocatalytic determination of epinephrine in the presence of p-chloranil as a mediator. J Solid State Electrochem 16(2):563–568
13. Ghica ME, Wintersteller Y, Brett CMA (2013) Poly(brilliant green)/carbon nanotube-modified carbon film electrodes and application as sensors. J Solid State Electrochem 17(6):1571–1580
14. Silva RM, Fernandes AJS, Ferro MC, Pinna N, Silva RF (2015) Vertically aligned N-doped CNTs growth using Taguchi experimental design. Appl Surf Sci 344:57–64
15. He CY, Shen PK (2013) Synthesis of the nitrogen-doped carbon nanotube (NCNT) bouquets and their electrochemical properties. Electrochem Commun 35:80–83
16. Xiao CH, Zou Q, Tang YH (2014) Surface nitrogen-enriched carbon nanotubes for uniform dispersion of platinum nanoparticles and their electrochemical biosensing property. Electrochim Acta 143: 10–17
17. Guo SY, Xu L, Xu BB, Sun ZX, Wang LH (2015) A ternary nanocomposite electrode of polyoxometalate/carbon nanotubes/gold nanoparticles for electrochemical detection of hydrogen peroxide. Analyst 140(3):820–826
18. Fernandes DM, Nunes M, Araujo MP (2016) Carbon nanomaterials-based modified electrodes for electrocatalysis. Bol Grupo Esp Carbon 40:3–8
19. Sosnowska M, Goral-Kurbiel M, Skunik-Nuckowska M, Jurczakowski R, Kulesza PJ (2013) Hybrid materials utilizing polyelectrolyte-derivatized carbon nanotubes and vanadium-mixed addenda heteropolytungstate for efficient electrochemical charging and electrocatalysis. J Solid State Electrochem 17(6): 1631–1640
20. Ji YC, Huang LJ, Hu J, Streb C, Song YF (2015) Polyoxometalate-functionalized nanocarbon materials for energy conversion, energy storage and sensor systems. Energy Environ Sci 8(3):776–789
21. Wang H, Kawasaki N, Yokoyama T, Yoshikawa H, Awaga K (2012) Molecular cluster batteries of nano-hybrid materials between Keggin POMs and SWNTs. Dalton Trans 41(33):9863–9866
22. Ji YC, Hu J, Huang LJ, Chen W, Streb C, Song YF (2015) Covalent attachment of Anderson-type polyoxometalates to single-walled carbon nanotubes gives enhanced performance electrodes for lithium ion batteries. Chem-Eur J 21(17):6469–6474
23. Chen W, Huang LJ, Hu J, Li TF, Jia FF, Song YF (2014) Connecting carbon nanotubes to polyoxometalate clusters for engineering high-performance anode materials. Phys Chem Chem Phys 16(36):19668–19673
24. Akter T, Hu KW, Lian K (2011) Investigations of multilayer polyoxometalates-modified carbon nanotubes for electrochemical capacitors. Electrochim Acta 56(14):4966–4971

25. Bajwa G, Genovese M, Lian K (2013) Multilayer polyoxometalates-carbon nanotube composites for electrochemical capacitors. ECS J Solid State Sci Technol 2(10):M3046–M3050
26. Fernandes DM, Freire C (2015) Carbon nanomaterial-phosphomolybdate composites for oxidative Electrocatalysis. ChemElectroChem 2(2):269–279
27. Li ZF, Chen JH, Pan DW, Tao WY, Nie LH, Yao SZ (2006) A sensitive amperometric bromate sensor based on multi-walled carbon nanotubes/phosphomolybdic acid composite film. Electrochim Acta 51(20):4255–4261
28. Fernandes DM, Barbosa ADS, Pires J, Balula SS, Cunha-Silva L, Freire C (2013) Novel composite material Polyoxovanadate@MIL-101(Cr): a highly efficient Electrocatalyst for ascorbic acid oxidation. ACS Appl Mater Interfaces 5(24):13382–13390
29. Fernandes DM, Granadeiro CM, de Sousa PMP, Grazina R, Moura JJG, Silva P, Paz FAA, Cunha-Silva L, Balula SS, Freire C (2014) SiW11Fe@ MIL-101(Cr) composite: a novel and versatile electrocatalyst. ChemElectroChem 1(8):1293–1300
30. Fernandes DM, Nunes M, Carvalho RJ, Bacsa R, Mbomekalle I-M, Serp P, Oliveira P, Freire C (2015) Biomolecules electrochemical sensing properties of a PMo11V@N-doped few layer graphene nanocomposite. Inorganics 3:178–193
31. Taei M, Shavakhi M, Hadadzadeh H, Movahedi M, Rahimi M, Habibollahi S (2015) Simultaneous determination of epinephrine, acetaminophen, and tryptophan using Fe2O3(0.5)/SnO2(0.5) nanocomposite sensor. J Appl Electrochem 45(2):185–195
32. Liu BD, Ouyang XQ, Ding YP, Luo LQ, Xu D, Ning YQ (2016) Electrochemical preparation of nickel and copper oxides-decorated graphene composite for simultaneous determination of dopamine, acetaminophen and tryptophan. Talanta 146:114–121
33. Mazloum-Ardakani M, Zokaie M, Khoshroo A (2015) Carbon nanotube electrochemical sensor based on and benzofuran derivative as a mediator for the determination of levodopa, acetaminophen, and tryptophan. Ionics 21(6):1741–1749
34. Raoof JB, Chekin F, Ojani R, Barari S, Anbia M, Mandegarzad S (2012) Synthesis and characterization of ordered mesoporous carbon as electrocatalyst for simultaneous determination of epinephrine and acetaminophen. J Solid State Electrochem 16(12):3753–3760
35. Ye DX, Xu YH, Luo LQ, Ding YP, Wang YL, Liu XJ (2012) LaNi0.5Ti0.5O3/CoFe2O4-based sensor for sensitive determination of paracetamol. J Solid State Electrochem 16(4):1635–1642
36. Fernandes DM, Silva N, Pereira C, Moura C, Magalhaes J, Bachiller-Baeza B, Rodriguez-Ramos I, Guerrero-Ruiz A, Delerue-Matos C, Freire C (2015) MnFe2O4@CNT-N as novel electrochemical nanosensor for determination of caffeine, acetaminophen and ascorbic acid. Sens Actuator B-Chem 218:128–136
37. Rajalakshmi K, John SA (2014) Sensitive and selective determination of L-tryptophan at physiological pH using functionalized multiwalled carbon nanotubes-nanostructured conducting polymer composite modified electrode. J Electroanal Chem 734:31–37
38. Keyvanfard M, Shakeri R, Karimi-Maleh H, Alizad K (2013) Highly selective and sensitive voltammetric sensor based on modified multiwall carbon nanotube paste electrode for simultaneous determination of ascorbic acid, acetaminophen and tryptophan. Mater Sci Eng C-Mater Biol Appl 33(2):811–816
39. Nasirizadeh N, Shekari Z, Zare HR, Shishehbore MR, Fakhari AR, Ahmar H (2013) Electrosynthesis of an imidazole derivative and its application as a bifunctional electrocatalyst for simultaneous determination of ascorbic acid, adrenaline, acetaminophen, and tryptophan at a multi-wall carbon nanotubes modified electrode surface. Biosens Bioelectron 41:608–614
40. Faba L, Criado YA, Gallegos-Suarez E, Perez-Cadenas M, Diaz E, Rodriguez-Ramos I, Guerrero-Ruiz A, Ordonez S (2013) Preparation of nitrogen-containing carbon nanotubes and study of their performance as basic catalysts. Appl Catal A-Gen 458:155–161
41. Himeno S, Ishio N (1998) A voltammetric study on the formation of V(V)- and V(IV)-substituted molybdophosphate(V) complexes in aqueous solution. J Electroanal Chem 451(1–2):203–209
42. Kong XK, Sun ZY, Chen M, Chen CL, Chen QW (2013) Metal-free catalytic reduction of 4-nitrophenol to 4-aminophenol by N-doped graphene. Energy Environ Sci 6(11):3260–3266
43. Kumarasinghe AR, Samaranayake L, Bondino F, Magnano E, Kottegoda N, Carlino E, Ratnayake UN, de Alwis AAP, Karunaratne V, Amaratunga GAJ (2013) Self-assembled multilayer graphene oxide membrane and carbon nanotubes synthesized using a rare form of natural graphite. J Phys Chem C 117(18):9507–9519
44. Lipinska ME, Rebelo SLH, Pereira MFR, Gomes J, Freire C, Figueiredo JL (2012) New insights into the functionalization of multi-walled carbon nanotubes with aniline derivatives. Carbon 50(9):3280–3294
45. Jang JW, Lee CE, Lyu SC, Lee TJ, Lee CJ (2004) Structural study of nitrogen-doping effects in bamboo-shaped multiwalled carbon nanotubes. Appl Phys Lett 84(15):2877–2879
46. Wang DW, Su DS (2014) Heterogeneous nanocarbon materials for oxygen reduction reaction. Energy Environ Sci 7(2):576–591
47. Liang XQ, Zhong J, Shi YL, Guo J, Huang GL, Hong CH, Zhao YD (2015) Hydrothermal synthesis of highly nitrogen-doped few-layer graphene via solid-gas reaction. Mater Res Bull 61:252–258
48. Sadakane M, Steckhan E (1998) Electrochemical properties of polyoxometalates as electrocatalysts. Chem Rev 98(1):219–237
49. Wang SF, Xie F, Hu RF (2007) Carbon-coated nickel magnetic nanoparticles modified electrodes as a sensor for determination of acetaminophen. Sens Actuator B-Chem 123(1):495–500
50. Amiri-Aref M, Raoof JB, Ojani R (2014) A highly sensitive electrochemical sensor for simultaneous voltammetric determination of noradrenaline, acetaminophen, xanthine and caffeine based on a flavonoid nanostructured modified glassy carbon electrode. Sens Actuator B-Chem 192:634–641
51. Barsan MM, Toledo CT, Brett CMA (2015) New electrode architectures based on poly(methylene green) and functionalized carbon nanotubes: characterization and application to detection of acetaminophen and pyridoxine. J Electroanal Chem 736:8–15
52. Ghica ME, Ferreira GM, Brett CMA (2015) Poly(thionine)-carbon nanotube modified carbon film electrodes and application to the simultaneous determination of acetaminophen and dipyrone. J Solid State Electrochem 19(9):2869–2881
53. Tsierkezos NG, Othman SH, Ritter U (2014) Nitrogen-doped carbon nanotubes modified with gold nanoparticles for simultaneous analysis of N-acetylcysteine and acetaminophen. J Solid State Electrochem 18(3):629–637